ACTA ASTRONOMICA
Vol. **52** (2002) pp. 217–240

The Optical Gravitational Lensing Experiment. *BVI* Maps of Dense Stellar Regions. III. The Galactic Bulge*

by

A. Udalski[1], M. Szymański[1], M. Kubiak[1],
G. Pietrzyński[1,2], I. Soszyński, P. Woźniak[3], K. Żebruń
O. Szewczyk[1] and Ł. Wyrzykowski[1]

[1] Warsaw University Observatory, Al. Ujazdowskie 4, 00-478 Warszawa, Poland
e-mail: (udalski,msz,mk,pietrzyn,soszynsk,zebrun,szewczyk,wyrzykow)@astrouw.edu.pl
[2] Universidad de Concepción, Departamento de Fisica, Casilla 160–C, Concepción, Chile
[3] Los Alamos National Laboratory, MS-D436, Los Alamos, NM 87545 USA
e-mail: wozniak@lanl.gov

Received September 17, 2002

ABSTRACT

We present the *VI* photometric maps of the Galactic bulge. They contain *VI* photometry and astrometry of about 30 million stars from 49 fields of 0.225 square degree each in the Galactic center region. The data were collected during the second phase of the OGLE microlensing project. We discuss the accuracy of data and present color-magnitude diagrams of selected fields observed by OGLE in the Galactic bulge.

The *VI* maps of the Galactic bulge are accessible electronically for the astronomical community from the OGLE Internet archive.

Key words: *Galaxy: bulge – Surveys – Catalogs – Techniques: photometric*

1. Introduction

Natural by-products of large microlensing surveys are huge photometric databases containing photometry of millions of stars from extremely interesting regions of the sky like the Galactic bulge, Galactic disk or Magellanic Clouds. These data may be used for many projects unrelated directly to microlensing. Long time baselines and very good accuracy of photometric data collected with modern CCD detectors make them a gold mine for stellar studies in both variable and non-variable domains. The list of possible projects is long and actually not limited to star research (Dobrzycki *et al.* 2002, Eyer 2002).

*Based on observations obtained with the 1.3 m Warsaw telescope at the Las Campanas Observatory of the Carnegie Institution of Washington.

The data collected during the second phase of the Optical Gravitational Lensing Experiment (OGLE-II, Udalski, Kubiak and Szymański 1997) are particularly attractive for many projects requiring precise photometry. Among the other datasets collected during the microlensing searches, only the OGLE photometry was obtained with the standard *BVI* filters what makes it very well suited for many astronomical projects. Also, very good astronomical site where the OGLE project has been conducted – the Las Campanas Observatory in Chile, made it possible to achieve the best resolution what is crucial in the very dense stellar fields like the Galactic bulge or Magellanic Clouds.

In the previous papers of the series the OGLE project released the photometric maps of the Small and Large Magellanic Clouds (Udalski *et al.* 1998, Udalski *et al.* 2000) which contained the mean *BVI* photometry and astrometry of more than 7 million and 2 million stars from the central parts of the LMC and SMC, respectively. These maps have been widely used by many astronomers worldwide for many projects (*e.g.*, Zaritsky *et al.* 2002, Edge and Coe 2002, Cordier *et al.* 2002, Subramaniam and Anupama 2002, Dobrzycki *et al.* 2002, Eyer 2002 and many more).

In this paper, which is a continuation of the series, we release "The OGLE *VI* Maps of the Galactic Bulge". The maps contain the mean *VI* photometry and astrometry of about 30 million stars from the fields covering about 11 square degrees in different parts of the Galactic center region.

Because of potentially great impact on many astrophysical fields, in particular for studying poorly observed stellar populations toward the Galactic bulge, the OGLE policy is to make the photometric data available to the wide astronomical community. Similarly to our previous maps, the maps of the Galactic bulge are also available from the OGLE Internet archive. Details are provided in the last Section of this paper.

2. Observations

Observations presented in this paper were collected during the second phase of the OGLE microlensing search with the 1.3-m Warsaw telescope at Las Campanas Observatory, Chile. The observatory is operated by the Carnegie Institution of Washington. The telescope was equipped with the "first generation" camera with a SITe 2048×2048 CCD detector working in drift-scan mode. The pixel size was 24 μm giving the 0.417 arcsec/pixel scale. Observations were performed in the "medium" reading mode of the CCD detector with the gain 7.1 e^-/ADU and readout noise of about 6.3 e^-. Details of the instrumentation setup can be found in Udalski, Kubiak and Szymański (1997).

Forty nine driftscan fields covering about 11 square degrees were monitored regularly (practically on every clear night) in the observing seasons 1997–2000. Each of the field covers 14.2×57 arcmin on the sky. Table 1 lists the equatorial

T a b l e 1

OGLE-II fields in the Galactic bulge

Field	RA (J2000)	DEC (J2000)	l	b
BUL_SC1	$18^h02^m32\overset{s}{.}5$	$-29°57'41''$	$1\overset{\circ}{.}08$	$-3\overset{\circ}{.}62$
BUL_SC2	$18^h04^m28\overset{s}{.}6$	$-28°52'35''$	$2\overset{\circ}{.}23$	$-3\overset{\circ}{.}46$
BUL_SC3	$17^h53^m34\overset{s}{.}4$	$-29°57'56''$	$0\overset{\circ}{.}11$	$-1\overset{\circ}{.}93$
BUL_SC4	$17^h54^m35\overset{s}{.}7$	$-29°43'41''$	$0\overset{\circ}{.}43$	$-2\overset{\circ}{.}01$
BUL_SC5	$17^h50^m21\overset{s}{.}7$	$-29°56'49''$	$-0\overset{\circ}{.}23$	$-1\overset{\circ}{.}33$
BUL_SC6	$18^h08^m03\overset{s}{.}7$	$-32°07'48''$	$-0\overset{\circ}{.}25$	$-5\overset{\circ}{.}70$
BUL_SC7	$18^h09^m10\overset{s}{.}6$	$-32°07'40''$	$-0\overset{\circ}{.}14$	$-5\overset{\circ}{.}91$
BUL_SC8	$18^h23^m06\overset{s}{.}2$	$-21°47'53''$	$10\overset{\circ}{.}48$	$-3\overset{\circ}{.}78$
BUL_SC9	$18^h24^m02\overset{s}{.}5$	$-21°47'55''$	$10\overset{\circ}{.}59$	$-3\overset{\circ}{.}98$
BUL_SC10	$18^h20^m06\overset{s}{.}6$	$-22°23'03''$	$9\overset{\circ}{.}64$	$-3\overset{\circ}{.}44$
BUL_SC11	$18^h21^m06\overset{s}{.}5$	$-22°23'05''$	$9\overset{\circ}{.}74$	$-3\overset{\circ}{.}64$
BUL_SC12	$18^h16^m06\overset{s}{.}3$	$-23°57'54''$	$7\overset{\circ}{.}80$	$-3\overset{\circ}{.}37$
BUL_SC13	$18^h17^m02\overset{s}{.}6$	$-23°57'44''$	$7\overset{\circ}{.}91$	$-3\overset{\circ}{.}58$
BUL_SC14	$17^h47^m02\overset{s}{.}7$	$-23°07'30''$	$5\overset{\circ}{.}23$	$2\overset{\circ}{.}81$
BUL_SC15	$17^h48^m06\overset{s}{.}9$	$-23°06'09''$	$5\overset{\circ}{.}38$	$2\overset{\circ}{.}63$
BUL_SC16	$18^h10^m06\overset{s}{.}7$	$-26°18'05''$	$5\overset{\circ}{.}10$	$-3\overset{\circ}{.}29$
BUL_SC17	$18^h11^m03\overset{s}{.}6$	$-26°12'35''$	$5\overset{\circ}{.}28$	$-3\overset{\circ}{.}45$
BUL_SC18	$18^h07^m03\overset{s}{.}5$	$-27°12'48''$	$3\overset{\circ}{.}97$	$-3\overset{\circ}{.}14$
BUL_SC19	$18^h08^m02\overset{s}{.}4$	$-27°12'45''$	$4\overset{\circ}{.}08$	$-3\overset{\circ}{.}35$
BUL_SC20	$17^h59^m19\overset{s}{.}1$	$-28°52'55''$	$1\overset{\circ}{.}68$	$-2\overset{\circ}{.}47$
BUL_SC21	$18^h00^m22\overset{s}{.}3$	$-28°51'45''$	$1\overset{\circ}{.}80$	$-2\overset{\circ}{.}66$
BUL_SC22	$17^h56^m47\overset{s}{.}6$	$-30°47'46''$	$-0\overset{\circ}{.}26$	$-2\overset{\circ}{.}95$
BUL_SC23	$17^h57^m54\overset{s}{.}5$	$-31°12'36''$	$-0\overset{\circ}{.}50$	$-3\overset{\circ}{.}36$
BUL_SC24	$17^h53^m17\overset{s}{.}9$	$-32°52'45''$	$-2\overset{\circ}{.}44$	$-3\overset{\circ}{.}36$
BUL_SC25	$17^h54^m26\overset{s}{.}1$	$-32°52'49''$	$-2\overset{\circ}{.}32$	$-3\overset{\circ}{.}56$
BUL_SC26	$17^h47^m15\overset{s}{.}5$	$-34°59'31''$	$-4\overset{\circ}{.}90$	$-3\overset{\circ}{.}37$
BUL_SC27	$17^h48^m23\overset{s}{.}6$	$-35°09'32''$	$-4\overset{\circ}{.}92$	$-3\overset{\circ}{.}65$
BUL_SC28	$17^h47^m05\overset{s}{.}8$	$-37°07'47''$	$-6\overset{\circ}{.}76$	$-4\overset{\circ}{.}42$
BUL_SC29	$17^h48^m10\overset{s}{.}8$	$-37°07'21''$	$-6\overset{\circ}{.}64$	$-4\overset{\circ}{.}62$
BUL_SC30	$18^h01^m25\overset{s}{.}0$	$-28°49'55''$	$1\overset{\circ}{.}94$	$-2\overset{\circ}{.}84$
BUL_SC31	$18^h02^m22\overset{s}{.}6$	$-28°37'21''$	$2\overset{\circ}{.}23$	$-2\overset{\circ}{.}94$
BUL_SC32	$18^h03^m26\overset{s}{.}8$	$-28°38'02''$	$2\overset{\circ}{.}34$	$-3\overset{\circ}{.}14$
BUL_SC33	$18^h05^m30\overset{s}{.}9$	$-28°52'50''$	$2\overset{\circ}{.}35$	$-3\overset{\circ}{.}66$
BUL_SC34	$17^h58^m18\overset{s}{.}5$	$-29°07'50''$	$1\overset{\circ}{.}35$	$-2\overset{\circ}{.}40$
BUL_SC35	$18^h04^m28\overset{s}{.}6$	$-27°56'56''$	$3\overset{\circ}{.}05$	$-3\overset{\circ}{.}00$
BUL_SC36	$18^h05^m31\overset{s}{.}2$	$-27°56'44''$	$3\overset{\circ}{.}16$	$-3\overset{\circ}{.}20$
BUL_SC37	$17^h52^m32\overset{s}{.}2$	$-29°57'44''$	$0\overset{\circ}{.}00$	$-1\overset{\circ}{.}74$
BUL_SC38	$18^h01^m28\overset{s}{.}0$	$-29°57'01''$	$0\overset{\circ}{.}97$	$-3\overset{\circ}{.}42$
BUL_SC39	$17^h55^m39\overset{s}{.}1$	$-29°44'52''$	$0\overset{\circ}{.}53$	$-2\overset{\circ}{.}21$
BUL_SC40	$17^h51^m06\overset{s}{.}1$	$-33°15'11''$	$-2\overset{\circ}{.}99$	$-3\overset{\circ}{.}14$
BUL_SC41	$17^h52^m07\overset{s}{.}2$	$-33°07'41''$	$-2\overset{\circ}{.}78$	$-3\overset{\circ}{.}27$
BUL_SC42	$18^h09^m05\overset{s}{.}0$	$-26°51'53''$	$4\overset{\circ}{.}48$	$-3\overset{\circ}{.}38$
BUL_SC43	$17^h35^m13\overset{s}{.}5$	$-27°11'00''$	$0\overset{\circ}{.}37$	$2\overset{\circ}{.}95$
BUL_SC44	$17^h49^m22\overset{s}{.}4$	$-30°02'45''$	$-0\overset{\circ}{.}43$	$-1\overset{\circ}{.}19$
BUL_SC45	$18^h03^m36\overset{s}{.}5$	$-30°05'00''$	$0\overset{\circ}{.}98$	$-3\overset{\circ}{.}94$
BUL_SC46	$18^h04^m39\overset{s}{.}7$	$-30°05'11''$	$1\overset{\circ}{.}09$	$-4\overset{\circ}{.}14$
BUL_SC47	$17^h27^m03\overset{s}{.}7$	$-39°47'16''$	$-11\overset{\circ}{.}19$	$-2\overset{\circ}{.}60$
BUL_SC48	$17^h28^m14\overset{s}{.}0$	$-39°46'58''$	$-11\overset{\circ}{.}07$	$-2\overset{\circ}{.}78$
BUL_SC49	$17^h29^m25\overset{s}{.}1$	$-40°16'21''$	$-11\overset{\circ}{.}36$	$-3\overset{\circ}{.}25$

coordinates of the center of each field and field acronym. Positions of some fields overlap by about one arcmin for testing purposes. The driftscan fields were selected to sample wide range ($-12^\circ < l < 12^\circ$) of the Galactic bulge regions. They were located typically in the strip of lower interstellar extinction below the Galactic equator at $b \approx -3^\circ$ in the areas of the highest stellar density. At positive galactic latitude low extinction windows are rare so only a few fields where the stellar density is high enough for microlensing search were selected. Fig. 1 presents the schematic map of the Galactic bulge with location of all OGLE-II bulge fields.

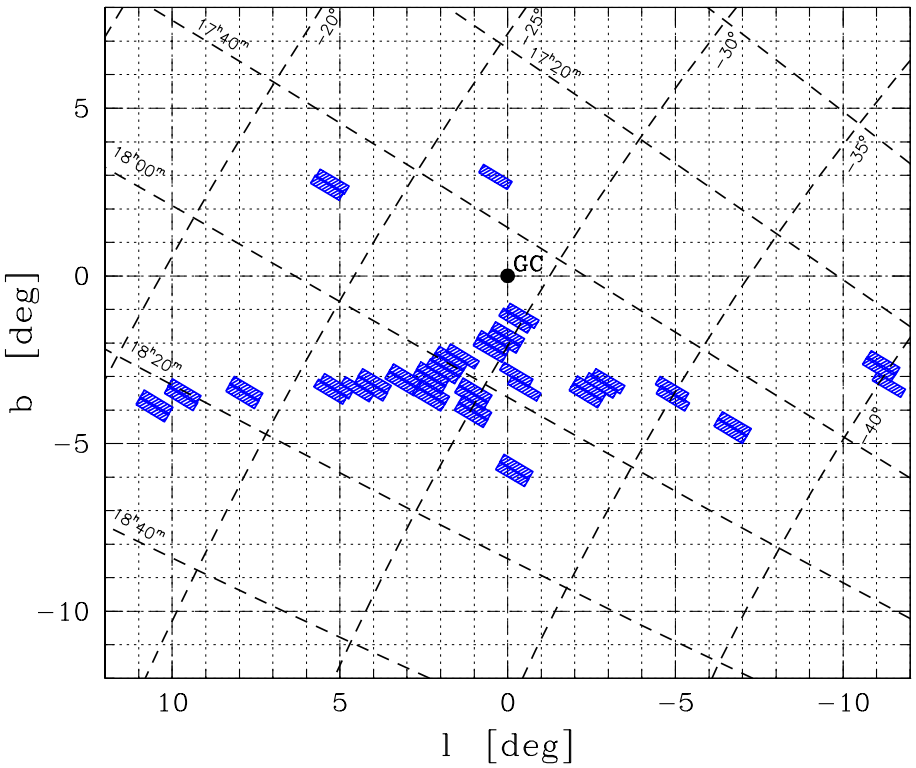

Fig. 1. OGLE-II fields in the Galactic bulge.

Regular observations of the Galactic bulge fields started on March 23, 1997 and continued up to November 23, 2000. Observations of three fields BUL_SC47, BUL_SC48 and BUL_SC49 began one year later in 1998 observing season. Two fields, namely BUL_SC45 and BUL_SC46 were observed less frequently mainly to maintain phasing of variable stars discovered in these fields during the OGLE-I phase. Photometry of part of BUL_SC45 field, based on much smaller observational material has already been presented in Paczyński *et al.* (1999).

Observations were obtained with the standard *VI* filters closely reproducing the standard system (Section 3). Due to the microlensing search observing strategy, the vast majority of observations were obtained through the *I*-band filter (150–570

per field) while much smaller number of frames in the *V*-band were collected (5–18). The effective exposure time was 87 and 124 seconds, for the *I* and *V*-band, respectively. After August 14, 1998 (HJD=2451040) the exposure time for the *I*-band was increased to 99.3 seconds.

More than 16 000 images (about 540 GB of raw data) of the Galactic bulge fields were collected during the OGLE-II phase of the OGLE survey. Because of high stellar density of the fields, observations were only conducted during the nights with good seeing conditions. The median seeing of the entire data set is about 1.25 arcsec. Observations were usually suspended when the seeing exceeded 1.6–1.8 arcsec.

3. Data Reduction and Calibration

All collected frames were reduced using the standard OGLE data pipeline in the identical manner as the SMC and LMC data (Udalski *et al.* 1998, Udalski *et al.* 2000). The data pipeline is described in detail in Udalski *et al.* (1998).

To summarize, after de-biasing and flat-fielding, photometry of objects was derived using the DOPHOT photometry program (Schechter, Saha and Mateo 1993) running in the fixed position mode on sixty four 512×512 pixel subframes. The driftscan image (2048×8192 pixels) was first matched with the so called "template" image, *i.e.*, the image with very good angular resolution (obtained at very good seeing conditions) and then divided into subframes. Photometry of each subframe was tied to the photometry of the template subframe by adding the mean shift derived usually from several hundreds bright stars. Thus, photometry of the template image defines the instrumental system. Objects detected in the template image for the *V*-band were first matched with the *I*-band template image objects of a given field so the star numbering was the same in all bands making the data handling much easier. Due to small shifts of the *V* template images in respect to the *I*-band image not all stars detected in the *I*-band image have *V* photometry.

To determine transformations of the instrumental photometry to the standard system, several Landolt (1992) standard fields were observed on about 250 photometric nights during the OGLE-II observations. Based on thousands observations of standard stars in Landolt (1992) fields located all over the sky and covering large range of colors (-0.2 mag $< V-I < 2$ mag), the following average transformations were derived:

$$\begin{aligned} V &= v - 0.002 \times (V-I) + \text{const}_V \\ I &= i + 0.029 \times (V-I) + \text{const}_I \\ V-I &= 0.969 \times (v-i) + \text{const}_{V-I} \end{aligned} \tag{1}$$

The typical residuals of calculated minus observed magnitudes of standard stars did not exceed 0.03 mag. Observations of standard stars indicate that the instrumental system was extremely stable during the period of observations and the standard

system magnitudes could be derived with good accuracy ($0.02 - 0.04$ mag) even during the photometric nights when no standard stars were observed.

Transformation of the instrumental magnitudes to the standard system was performed in the following steps. First, the aperture corrections were determined on each of the 64 subframes. They were derived from aperture photometry of typically 20–100 stars per subframe measured in images with faint stars subtracted. Then the total correction consisting of the aperture correction, zero point of transformation, extinction correction and normalization to 1 sec exposure time was obtained. The total corrections were derived independently for about 5 and 30–40 photometric nights for the V and I-band, respectively. Typical standard deviation of the total correction in each of the 64 subframes was of about 0.02–0.03 mag. The mean values of the total correction were subsequently used for the construction of photometric databases (Szymański and Udalski 1993, Udalski *et al.* 1998) for the V and I-band. The databases contain entire photometry of all objects in a given OGLE field in the system very close to the standard one – only the color term (Eq. 1) is not included.

Equatorial coordinates of objects detected in the OGLE fields were determined in the identical manner as described in Udalski *et al.* (1998). Objects in the OGLE-II frames were cross-identified with the objects detected in the Digitized Sky Survey images, and the transformation between the OGLE pixel grid and (RA,DEC) coordinates in the DSS coordinate system was derived. About 2000–14000 stars were used for transformation depending on the stellar density in the field. The internal accuracy of the determined equatorial coordinates, as measured in the overlapping regions of neighboring fields is about 0.15–0.20 arcsec. However we remind that the systematic error of the DSS coordinate system may reach 0.7 arcsec.

4. Accuracy of Transformation

As we mentioned in the previous Section the OGLE instrumental photometric data were tied to the standard Landolt (1992) system. While the derived transformations (Eq. 1) indicate close approximation of the Landolt's system it should be noted that the color range of observed standard stars was limited to $V - I < 2$ mag. For redder stars the transformations become extrapolation and are prone to systematic errors. While such systematic effects were negligible in the case of the OGLE-II maps of the Magellanic Clouds, because the vast majority of stars were bluer than $V - I \approx 2$ mag the situation is different in the Galactic bulge case. Many Galactic bulge fields are severely reddened due to large interstellar extinction toward the Galactic center and in some of the fields even more than 50% stars have $V - I > 2$ mag.

One of the main source of systematic errors could be different transmission of the OGLE filters compared to the standard system definition. While the V-band filter is a standard combo of Schott glass filters used to reproduce the V-band with

CCD detectors (Bessell 1990) and it should not introduce any significant systematic errors, the *I*-band filter is our main concern. OGLE-II used 4-mm RG9 Schott glass filter for *I*-filter approximation which is an alternative to the usually used interference filters (Bessell 1990). The glass filter replacement has wider long-wavelength wing, that is defined by CCD detector sensitivity, contrary to the much sharper drop of transmission at about 9000 Å of the standard *I* pass-band defined either by interference filter or by fall of sensitivity of photomultipliers originally used for definition of the *I*-band (Bessell 1990, Landolt 1992). Although this excess of red-side sensitivity of glass filter is rapidly falling with wavelength it can cause some non-linearities in transformations to the standard system, especially for very red objects or highly reddened by interstellar extinction regular stars. The latter are quite common in the Galactic bulge.

Moreover, the excess of the red sensitivity of OGLE-II filter can be affected by atmospheric transmission. In the range 9000–9900 Å the atmospheric transmission is reduced by telluric absorption bands. The amount of telluric absorption varies with the zenith distance and the amount of precipitable water vapor. This effect makes the OGLE-II filter closer to the standard one, but on the other hand, more sensitive to atmospheric conditions. Fortunately, at very good observing site like Las Campanas Observatory the atmospheric conditions are very stable in long term scale and the large number of photometric nights when calibrations were performed averages atmospheric condition fluctuations.

Ideally, one should determine differences between the OGLE-II and standard *I*-band filters by observing large number of red color standards. Unfortunately, the number of red standards is very limited and it is practically impossible to calibrate reliably the filters up to $V-I \approx 4$ mag. In practice, the reddest stars in the Landolt's (1992) standard fields observed by OGLE-II reached only $V-I \approx 2$ mag. Therefore to estimate the possible systematic errors for very red stars we calculated and compared expected *I*-band magnitudes for OGLE-II and standard filters using models of atmospheres by Kurucz (1993).

First, we derived the OGLE-II *I*-filter transmission curve using Schott glass filter catalog data and OGLE-II CCD detector quantum efficiency curve from manufacturer data sheet. It is shown in the upper panel of Fig. 2 with the transmission curve of the standard *I*-band filter as defined by Landolt (1992). We assumed full atmospheric transmission, so our further results are an upper limit of possible filter differences. As we mentioned above telluric absorption makes the filter transmissions more similar. It is known that both – the filter transmission and CCD sensitivity – can vary by a few percent from the catalog data. Therefore we additionally performed further calculations for transmission different by 5% from that shown in Fig. 2. In both cases results were practically identical.

We selected a typical red clump giant star for modeling. Such a star has $V-I \approx 1.0$ mag *i.e.*, its color is more or less in the middle of the range calibrated by standards ($V-I < 2$ mag). We took the Kurucz's model of atmosphere of a

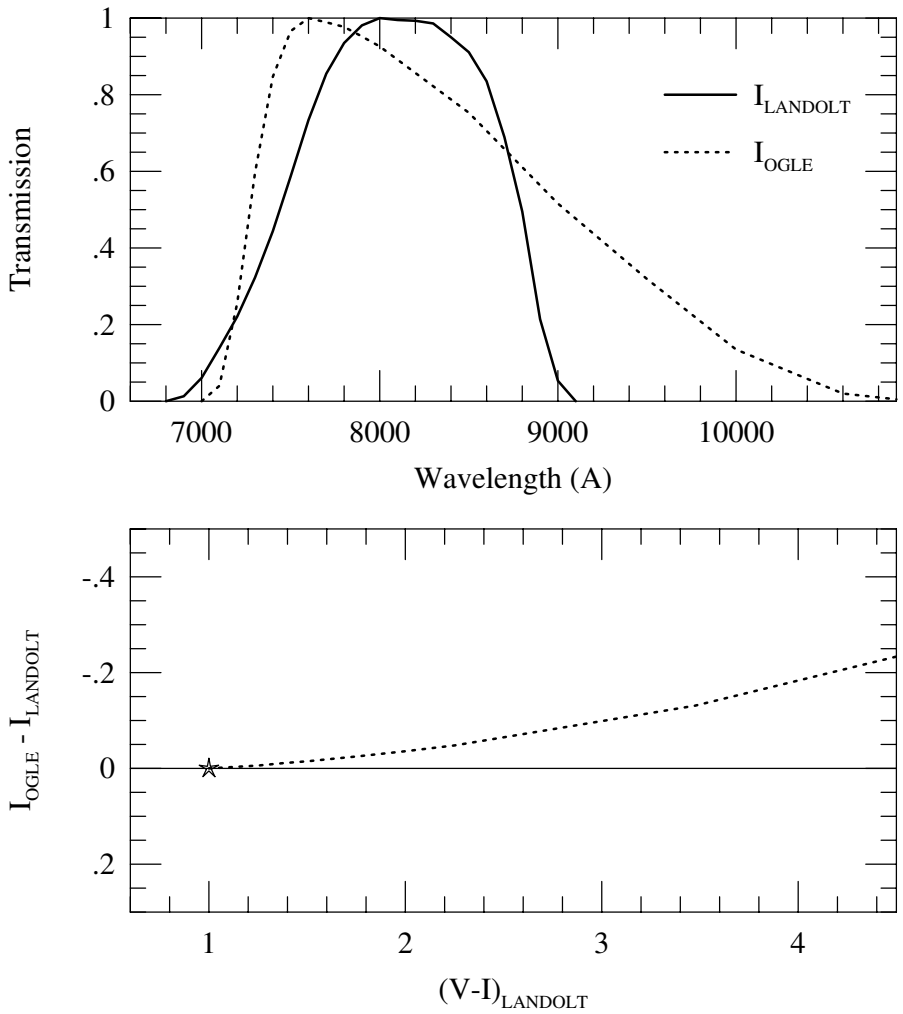

Fig. 2. *Upper panel*: dotted line – transmission of the OGLE-II *I*-band filter; solid line – transmission of the standard *I*-band filter according to Landolt (1992). *Lower panel*: Difference between OGLE-II filter magnitudes transformed to the Landolt's system with Eq. (1) and Landolt's standard *I*-band filter magnitudes (dotted line) for typical red clump giant (asterisk) reddened by standard extinction law.

giant with metallicity of $[\mathrm{Fe/H}] = -0.2$ (typical for Galactic bulge), $\log g = 2.00$ and $T_{\rm eff} = 4500$ K – typical red clump giant values. We used somewhat modified COUSINS.FOR program from the Kurucz's archive to determine the *I*-band magnitudes for such a giant star for OGLE-II and standard Landolt's *I*-band filter. Then we repeated calculations making the star redder by introducing the interstellar extinction obeying standard extinction law with $R_V = 3.1$ (Cardelli, Clayton and Mathis 1989). Calculations were performed up to very high reddening values of $E(B-V) = 3.0$ mag. The OGLE-II filter results were then transformed to the Landolt's system using our empirical transformations given by Eq. (1).

Lower panel of Fig. 2 presents results of our calculations. Asterisk marks position of unreddened red clump giant. Dotted line indicates the calculated difference of the OGLE-II filter values transformed to the Landolt's system with Eq. (1) transformations and magnitudes obtained for the Landolt's pass-band. As we expected, in the range covered by standard stars ($V-I<2$ mag) consistency of both magnitudes is very good at 0.03 mag level. However, for redder objects there is a systematic trend giving brighter *I*-band magnitudes (and redder $V-I$ colors) for the OGLE-II filter. This effect may reach 0.25 mag at very red $V-I>4$ mag stars and it is fully understandable, as for redder stars the red excess of the OGLE-II filter transmission is not fully compensated by linear transformation (Eq. 1) based on much bluer stars.

In practice, the differences presented in the lower panel of Fig. 2 are likely to be an upper limit of possible discrepancy between the OGLE-II and Landolt's standard system. For instance, it is likely that due to telluric absorption the real discrepancy is smaller. Because we are not able to determine precise empirical transformation to the Landolt system in the entire range of observed colors in the Galactic bulge, we leave the data transformed with Eq. (1). The reader should be, however, aware that for very red stars ($V-I>2$ mag) the magnitudes presented in the OGLE-II maps of the Galactic bulge can differ from the Landolt's system values even as much as presented in Fig. 2.

5. *VI* Maps of the Galactic Bulge

The *VI* maps of the Galactic bulge were constructed using the photometric databases of each field. First, the mean magnitudes of each object were calculated with 5σ clipping alghoritm. Then, we corrected the magnitudes for a small systematic error, caused by non-perfect flat-fielding at the edges of the field. This effect was first noticed by Dr. D.S. Graff (Ohio State University), and it was precisely mapped based on observations of hundreds of standard stars. Finally, the color corrections (Eq. 1) were derived and added. Only objects with more than 50 good observations (see Udalski *et al.* 1998) in the *I*-band were included in the final maps of the Galactic bulge. The errors of zero points of photometry should not exceed 0.04 mag. Table 2 lists the total number of objects in the OGLE-II maps of the Galactic bulge fields.

Table 3 presents the sample data from the map of the BUL_SC1 field. In the consecutive columns the following data are provided: star ID number, equatorial coordinates, (X,Y) coordinates in the *I*-band template image, photometry: *V*, $(V-I)$, *I*, number of observations, number of rejected observations and standard deviation for the *VI*-bands, respectively. In the electronic version we additionally provide the FITS template images for easy object identification. Maps of all Galactic bulge fields are available electronically from the OGLE Internet archive (see Section 8).

T a b l e 2

Number of objects in the OGLE-II Galactic bulge maps

Field	$N_{\rm objects}$	Field	$N_{\rm objects}$
BUL_SC1	729852	BUL_SC26	728200
BUL_SC2	803269	BUL_SC27	690785
BUL_SC3	805587	BUL_SC28	405799
BUL_SC4	774091	BUL_SC29	491941
BUL_SC5	433990	BUL_SC30	762481
BUL_SC6	514084	BUL_SC31	790471
BUL_SC7	462748	BUL_SC32	797493
BUL_SC8	401813	BUL_SC33	738508
BUL_SC9	330338	BUL_SC34	960656
BUL_SC10	458816	BUL_SC35	770940
BUL_SC11	425984	BUL_SC36	873472
BUL_SC12	534720	BUL_SC37	664424
BUL_SC13	569850	BUL_SC38	710234
BUL_SC14	619028	BUL_SC39	784316
BUL_SC15	600787	BUL_SC40	630774
BUL_SC16	699804	BUL_SC41	603404
BUL_SC17	687019	BUL_SC42	600519
BUL_SC18	749265	BUL_SC43	474367
BUL_SC19	732089	BUL_SC44	318561
BUL_SC20	785317	BUL_SC45	627412
BUL_SC21	882518	BUL_SC46	551815
BUL_SC22	715301	BUL_SC47	300705
BUL_SC23	723687	BUL_SC48	286907
BUL_SC24	612189	BUL_SC49	251629
BUL_SC25	622326		
		Total:	30490285

It is worth noting that although the maps contain only the mean photometry of detected stars they can also be used for discrimination of variable stars. Large standard deviation of *I*-band magnitudes usually indicates stellar variability. It should be also noted that the preliminary catalog of about 200 000 variable stars found in the OGLE-II Galactic bulge fields has already been released (Woźniak *et al.* 2002; it is also available from the OGLE Internet archive). The maps can be used for more accurate calibration of light curves from that catalog. As the numbering of objects is different in both catalogs, cross-identification can be done by comparison of pixel or equatorial coordinates (the pixel coordinates system is the same in both catalogs).

Table 3

Sample of data from the *VI* map of the field BUL_SC1

Star no	RA (J2000)	DEC (J2000)	X	Y	V	$V-I$	I	N^V_{ok}	N^V_{bad}	σ_V	N^I_{ok}	N^I_{bad}	σ_I
1	$18^h02^m13^s.55$	$-30°25'52''.6$	436.71	6.63	14.702	1.842	12.857	9	0	0.011	134	1	0.018
2	$18^h02^m13^s.25$	$-30°25'50''.3$	427.20	12.09	14.272	1.845	12.423	11	0	0.011	153	2	0.014
3	$18^h02^m07^s.46$	$-30°25'25''.4$	245.93	72.10	14.430	2.350	12.076	10	0	0.012	218	0	0.014
4	$18^h02^m05^s.04$	$-30°25'24''.8$	170.42	73.28	14.597	2.206	12.388	10	0	0.014	205	0	0.013
5	$18^h02^m06^s.55$	$-30°25'02''.5$	217.51	127.31	16.786	4.338	12.440	11	0	0.123	207	0	0.066
6	$18^h02^m12^s.63$	$-30°25'00''.1$	407.44	133.55	18.150	5.070	13.072	11	0	0.222	217	0	0.102
7	$18^h02^m11^s.18$	$-30°24'56''.7$	362.03	141.64	15.598	3.058	12.535	9	1	0.023	223	2	0.015
8	$18^h02^m07^s.45$	$-30°24'54''.9$	245.59	145.67	16.275	4.049	12.218	11	0	0.059	212	0	0.025
9	$18^h02^m11^s.38$	$-30°24'52''.6$	368.36	151.45	15.343	3.322	12.015	10	0	0.101	215	0	0.054
10	$18^h02^m03^s.26$	$-30°24'47''.6$	114.56	163.08	14.999	3.369	11.624	11	0	0.070	210	0	0.031
11	$18^h02^m00^s.00$	$-30°24'47''.3$	12.71	163.60	–	–	12.666	0	0	–	111	3	0.012
12	$18^h02^m15^s.40$	$-30°24'36''.2$	493.86	191.32	18.808	5.679	13.118	6	0	0.072	207	0	0.073
13	$18^h02^m04^s.24$	$-30°24'29''.0$	144.92	207.99	14.200	2.561	11.633	10	0	0.040	219	0	0.027
14	$18^h02^m01^s.05$	$-30°24'15''.6$	45.27	240.22	–	–	11.950	0	0	–	166	0	0.009
15	$18^h02^m08^s.06$	$-30°24'08''.8$	264.47	257.18	15.898	2.873	13.020	10	0	0.018	219	0	0.014
16	$18^h02^m00^s.65$	$-30°24'07''.2$	32.53	260.56	–	–	12.531	0	0	–	152	0	0.012
17	$18^h02^m03^s.60$	$-30°24'07''.4$	124.85	260.36	16.662	3.715	12.940	10	0	0.155	219	0	0.015
18	$18^h02^m13^s.46$	$-30°23'56''.6$	433.13	287.02	16.145	3.402	12.736	11	0	0.033	230	0	0.020
19	$18^h02^m03^s.70$	$-30°23'44''.5$	127.99	315.63	14.878	2.571	12.304	11	0	0.040	215	0	0.015
20	$18^h02^m02^s.05$	$-30°23'42''.8$	76.14	319.50	–	–	11.544	0	0	–	196	0	0.014
21	$18^h02^m06^s.93$	$-30°23'33''.1$	228.74	343.38	15.258	2.613	12.641	11	0	0.017	218	0	0.013
22	$18^h02^m02^s.41$	$-30°23'24''.2$	87.39	364.53	–	–	11.738	0	0	–	207	0	0.054

6. Data Tests

6.1. Photometry

Quality of the OGLE-II photometry can be assessed from comparison of magnitudes of stars located in the overlaps between neighboring fields. Because each of the fields was calibrated independently such a comparison provides informa-

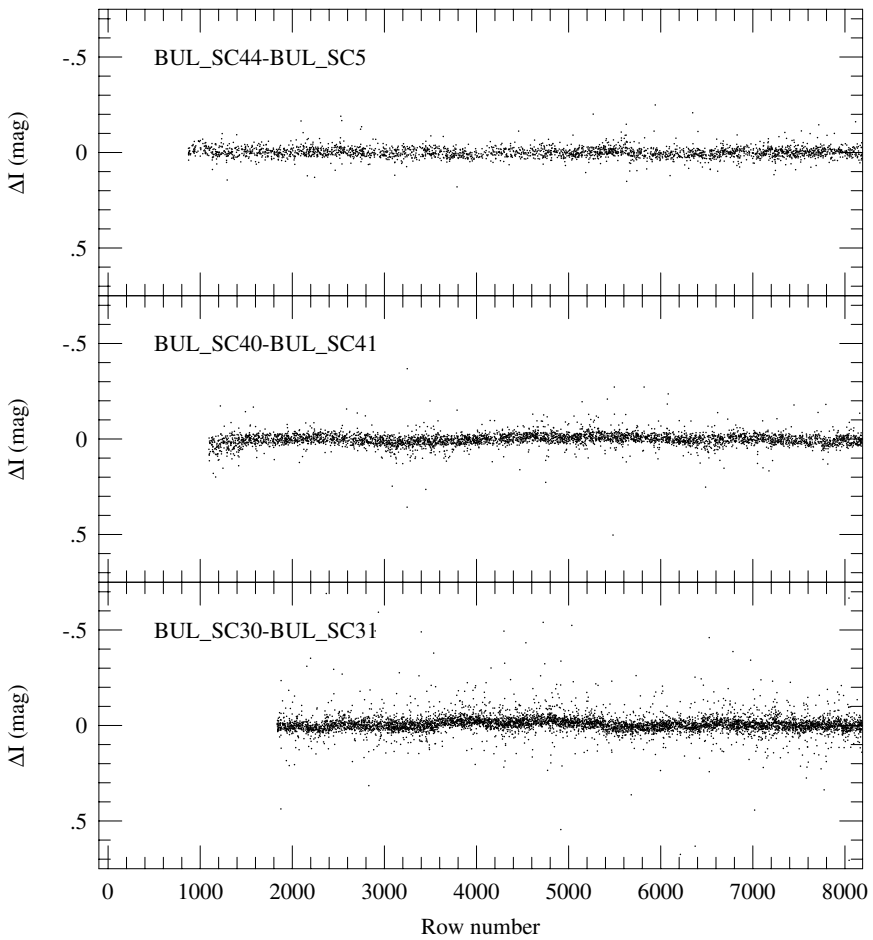

Fig. 3. Differences of magnitudes of the same objects in the overlapping regions of fields of low (upper panel), medium (middle panel) and high (bottom panel) stellar density in the *I*-band filter.

tion on accuracy of calibration and the typical accuracy of photometry. Figs. 3 and 4 present differences of magnitudes for stars with magnitudes brighter than $I = 17$ mag and $V = 19$ mag, plotted as a function of line number for three fields of different stellar density. The average difference of magnitudes is typically below 0.01 mag indicating good consistency of the calibration procedure. The typical sigma of the Gaussian fitted to the histogram of differences of magnitudes is about 0.025 mag for both, the *V* and *I*-band.

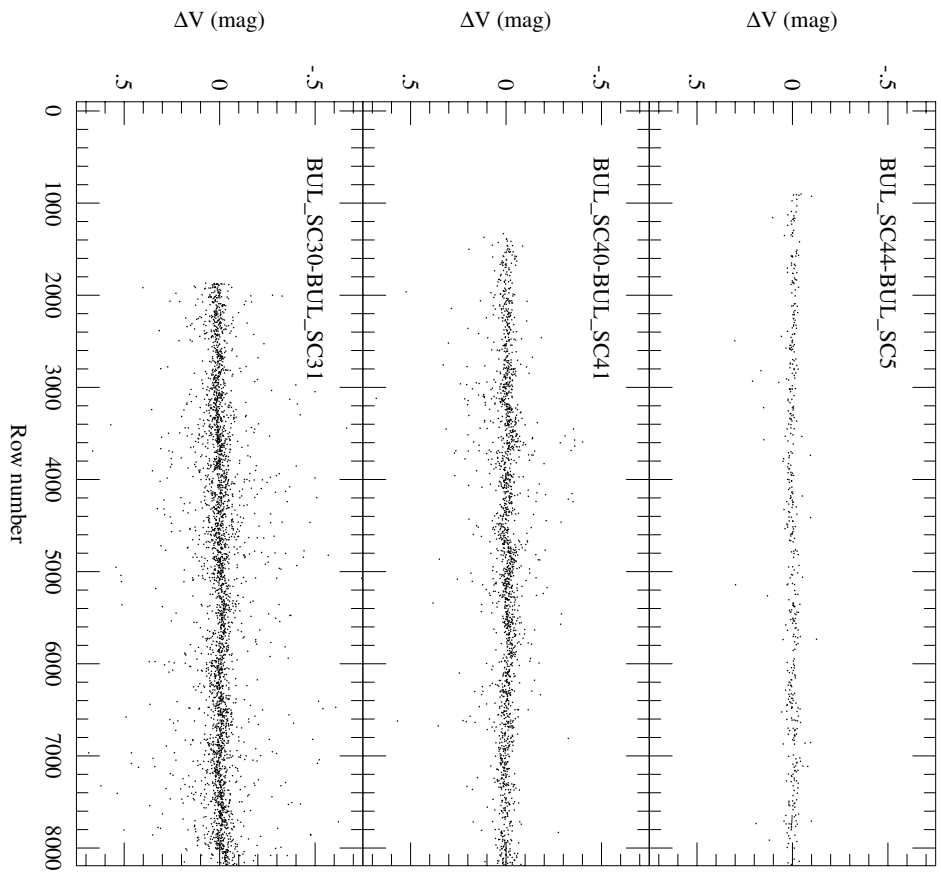

Fig. 4. Same as Fig. 4 for the *V*-band filter.

The error of photometric measurements as a function of stellar magnitude is shown in Figs. 5 and 6. Fig. 5 presents the standard deviation of *V* and *I*-band magnitudes of objects in the most crowded field BUL_SC34 while Fig. 6 in the rlatively little crowded field BUL_SC44.

6.2. Completeness

To estimate the completeness of detection of stars in the OGLE fields we performed similar set of tests as in the case of the SMC and LMC maps. For details the reader is referred to Udalski *et al.* (1998). In short, we selected a 512×512 pixel subframe of the tested field and added artificial stars in random locations. Their magnitude distribution is provided in the first column of Table 4. The subframe was then reduced by the standard reduction procedure and completeness of recovering the artificial stars was studied. One hundred such tests were performed for each subframe.

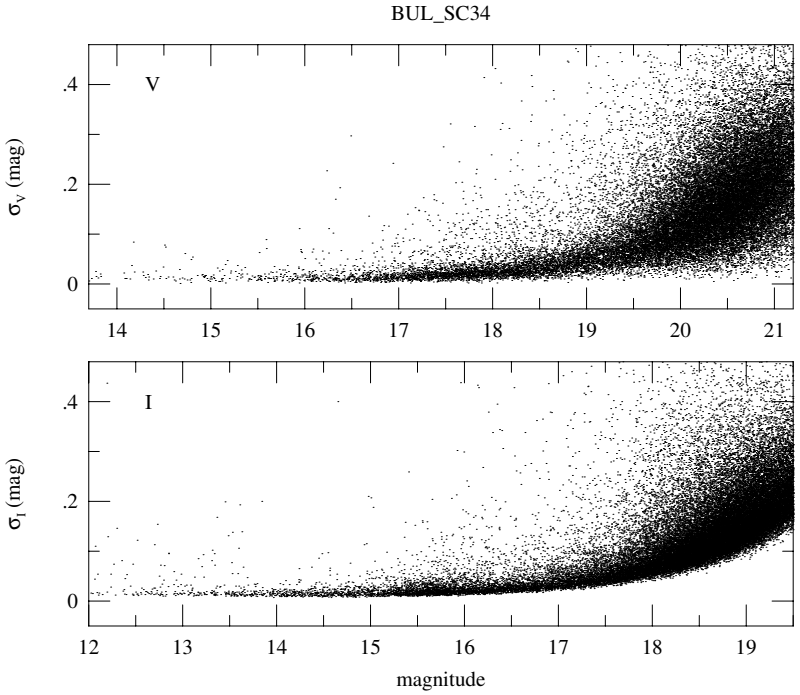

Fig. 5. Standard deviation as a function of magnitude for *V* and *I*-band in the highest density field BUL_SC34.

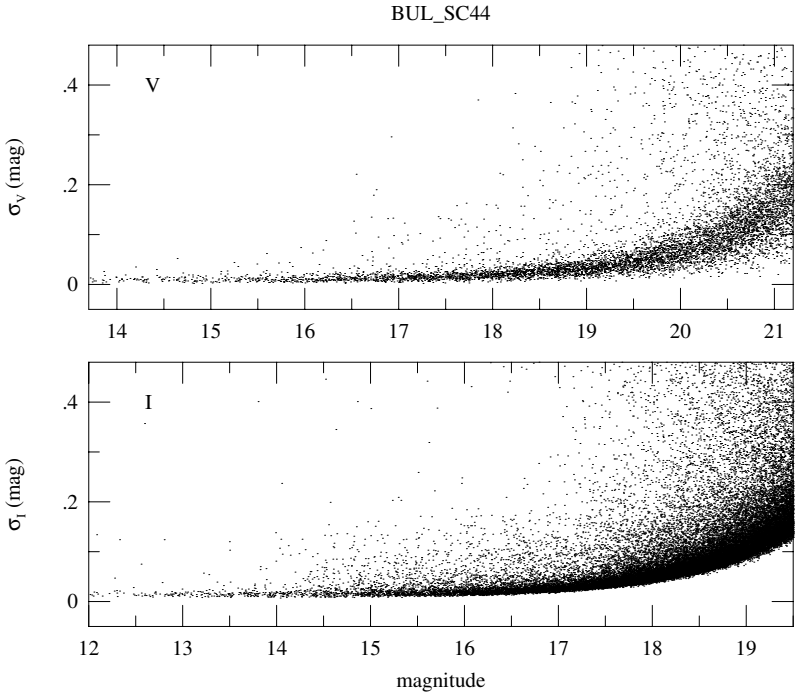

Fig. 6. Standard deviation as a function of magnitude for *V* and *I*-band in the low density field BUL_SC44.

Table 4 presents results of these tests for three fields of different stellar density for *I*-band. As can be seen the completeness is high down to stars as faint as $I \approx 18.0$ mag. For fainter stars it gradually drops. The completeness is also a strong function of stellar density of the field.

T a b l e 4

Completeness of the Galactic bulge maps

Stars		Completeness		
per bin	I	SC_34	SC_40	SC_44
2	12.8	99.0	98.5	99.5
5	13.3	98.4	99.8	99.2
7	13.8	96.1	99.1	98.7
10	14.3	97.4	99.2	98.8
12	14.8	96.2	98.7	98.4
15	15.3	96.8	98.6	99.1
17	15.8	94.8	98.1	98.4
20	16.3	93.8	96.5	97.9
22	16.8	91.4	96.0	97.3
25	17.3	87.4	94.0	96.3
27	17.8	79.8	91.2	93.6
30	18.3	67.3	85.2	91.0
32	18.8	48.5	75.5	86.9
35	19.3	26.9	56.9	80.0

7. Color-Magnitude Diagrams

Figs. 7–13 show *I vs.* $(V - I)$ color-magnitude diagrams (CMDs) of selected Galactic bulge fields. We present these diagrams to illustrate quality of data and potential usefulness of the OGLE-II maps for studying properties of the Galactic bulge populations. Only part of stars (*i.e.*, about 10–30% of the total number, depending on the field) from each field are plotted in these figures for clarity.

The CMDs in Figs. 7–13 clearly show the most characteristic features of stellar populations toward the Galactic center regions: the main sequence of disk stars (long almost vertical strip at blue side of the CMD), Galactic bulge red giant branch (vertical strip at red part of the CMD) with prominent red clump, Galactic bulge main sequence turn-off part etc.

Figs. 7–13 also show how severely the interstellar extinction affects the diagrams. In Fig. 7 CMDs of two fields located closest (about $1.^{\circ}25$) to the Galactic center are plotted. In BUL_SC44 field the interstellar extinction is so high that

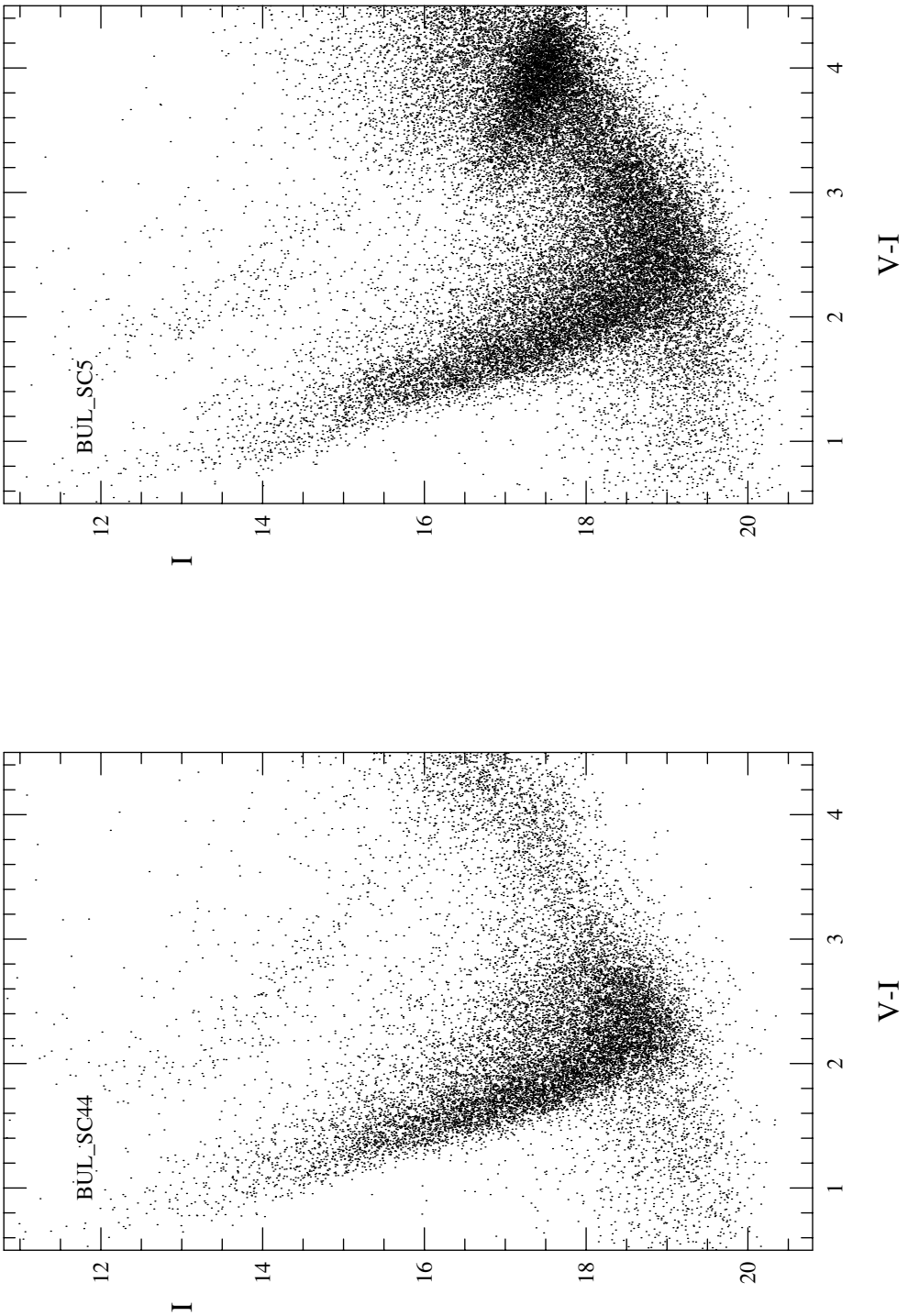

Fig. 7. Color-magnitude diagrams of the fields BUL_SC44 and BUL_SC5.

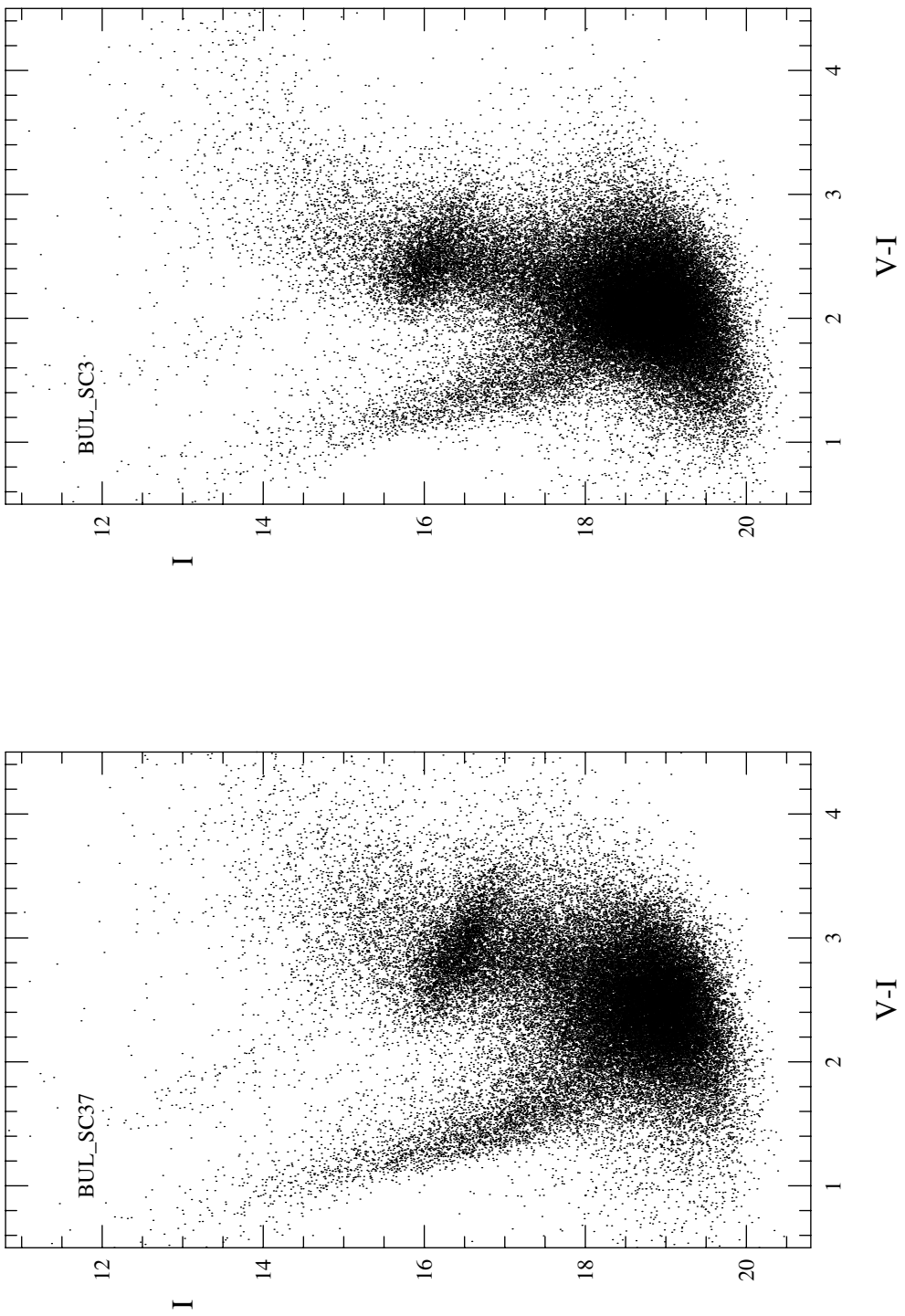

Fig. 8. Color-magnitude diagrams of the fields BUL_SC37 and BUL_SC3.

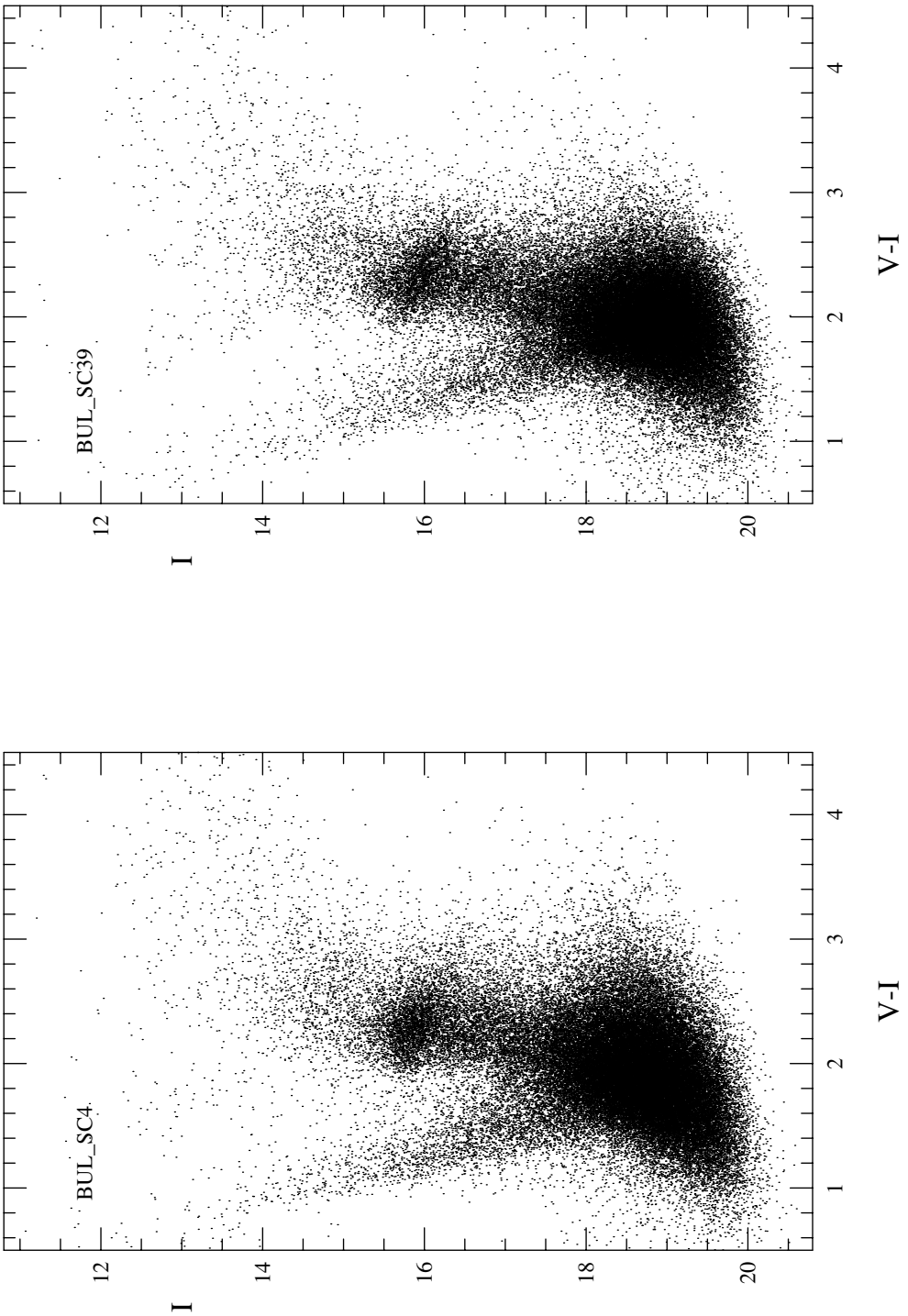

Fig. 9. Color-magnitude diagrams of the fields BUL_SC4 and BUL_SC39.

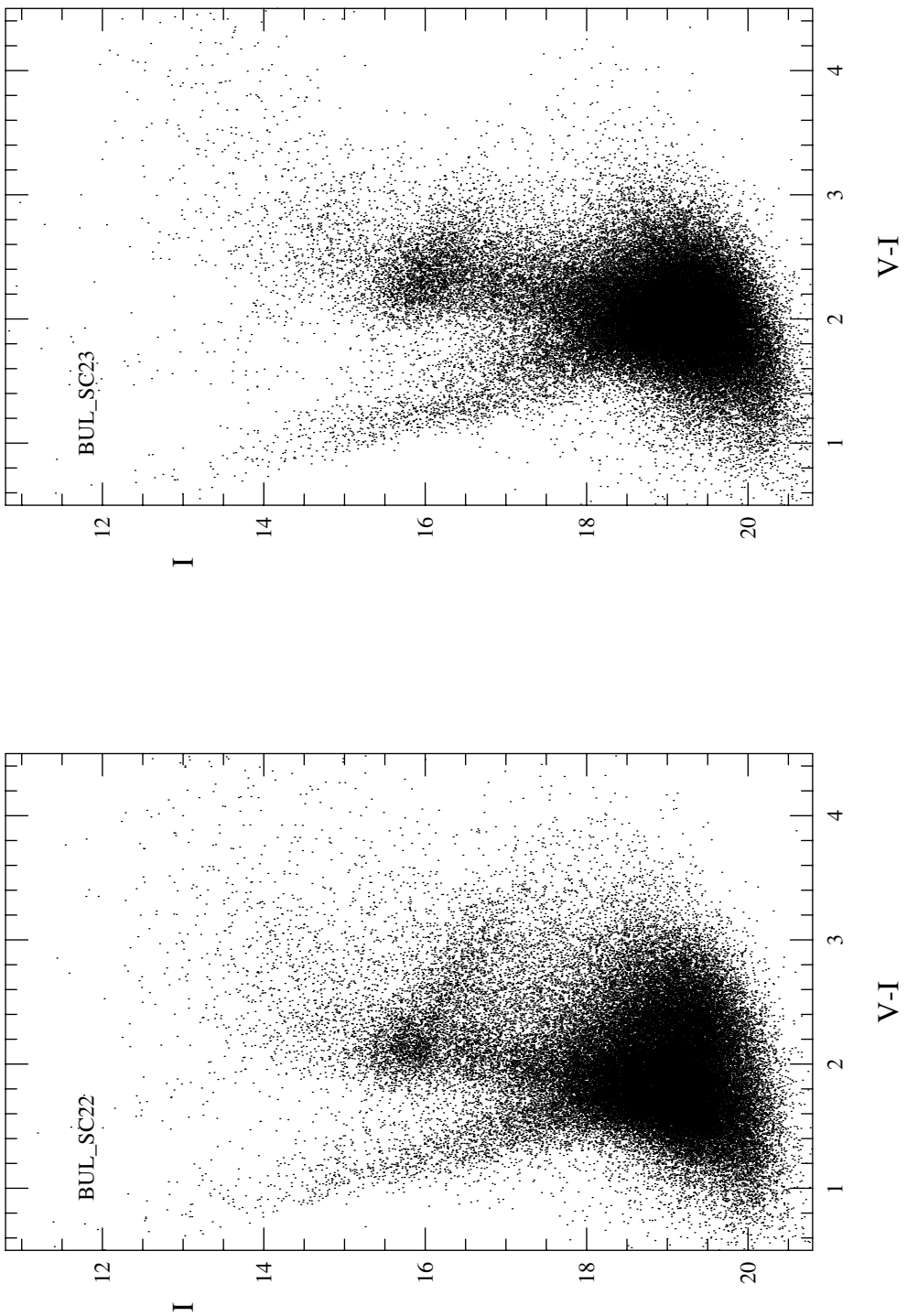

Fig. 10. Color-magnitude diagrams of the fields BUL_SC22 and BUL_SC23.

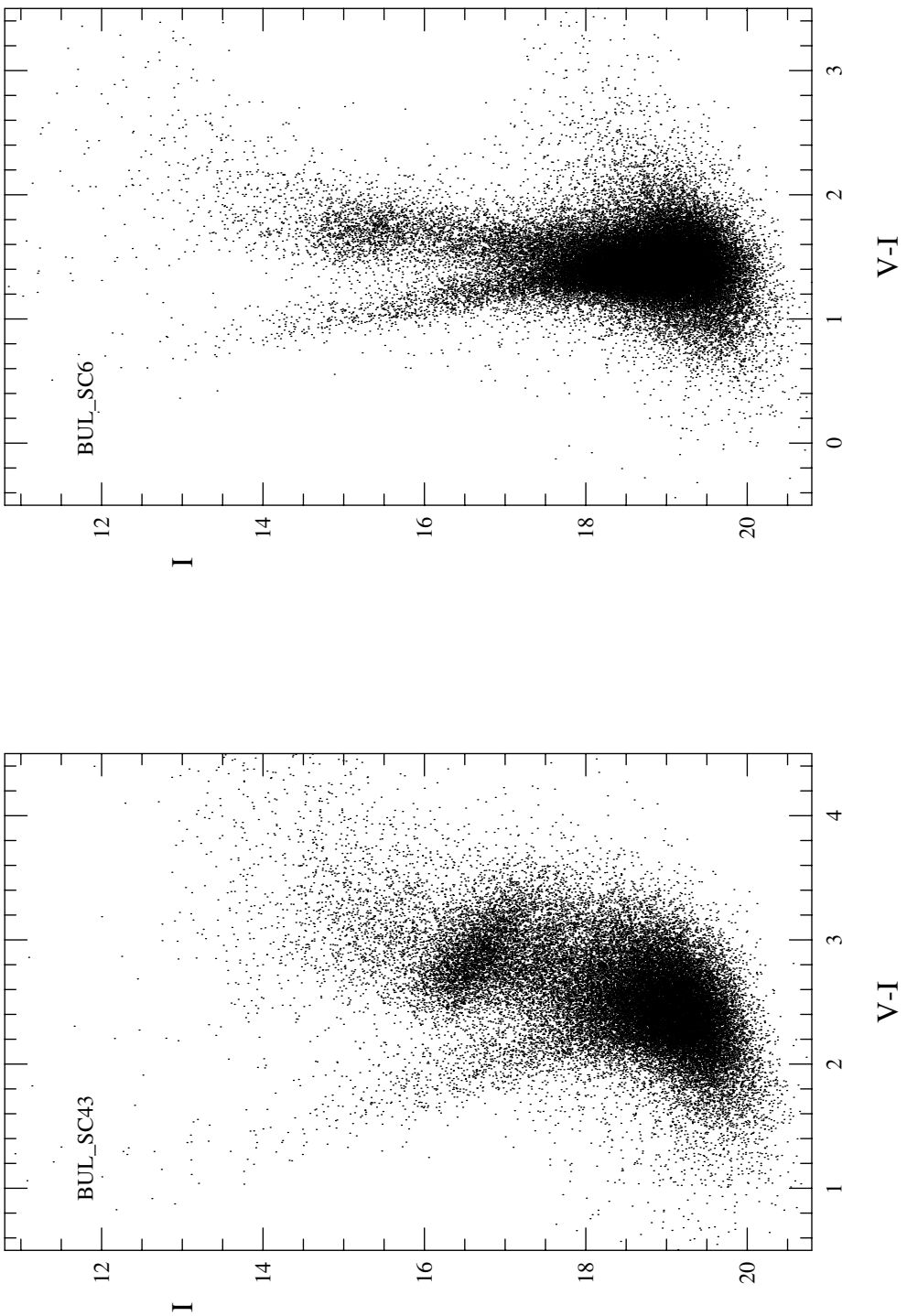

Fig. 11. Color-magnitude diagrams of the fields BUL_SC43 and BUL_SC6.

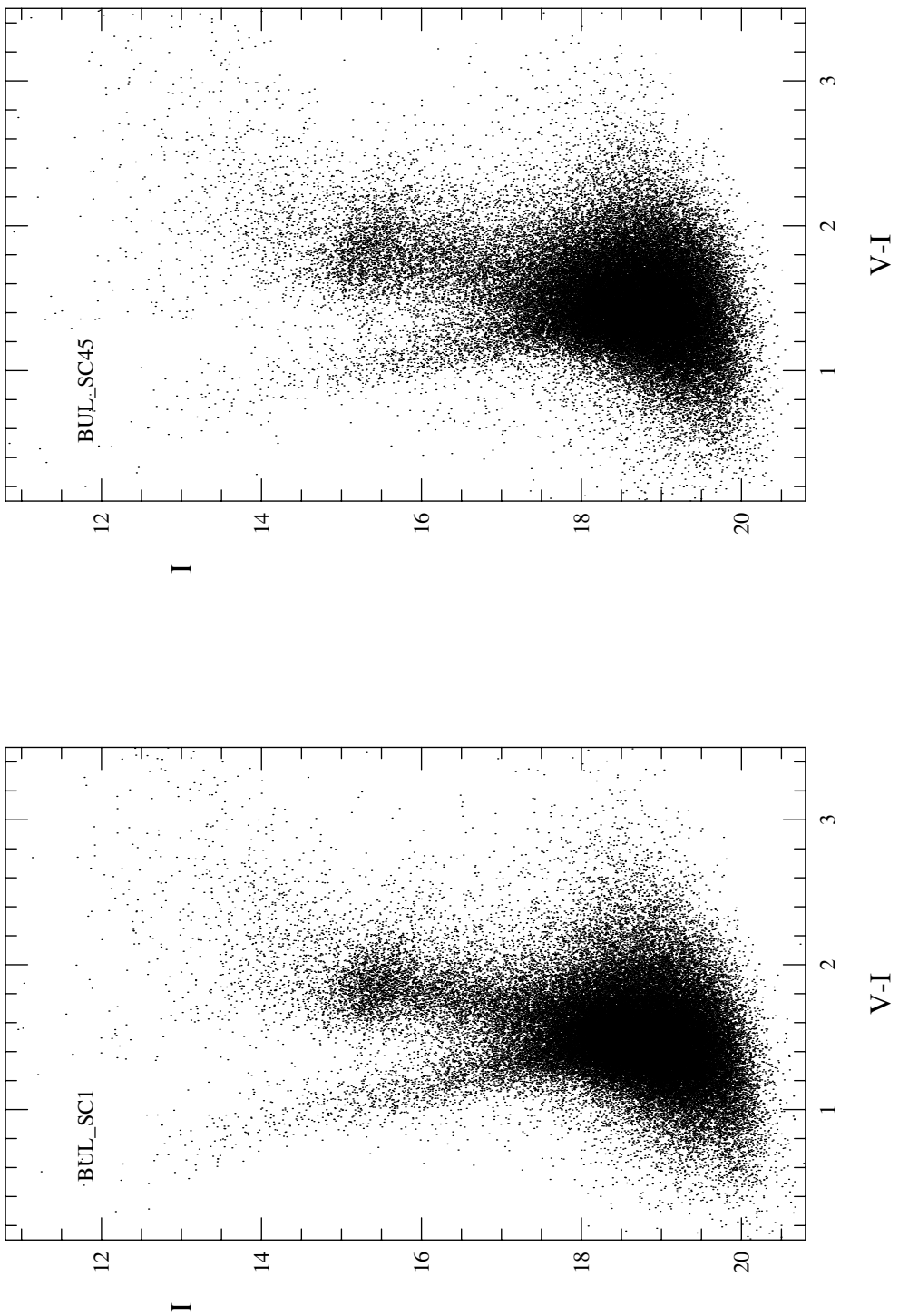

Fig. 12. Color-magnitude diagrams of the fields BUL_SC1 and BUL_SC45.

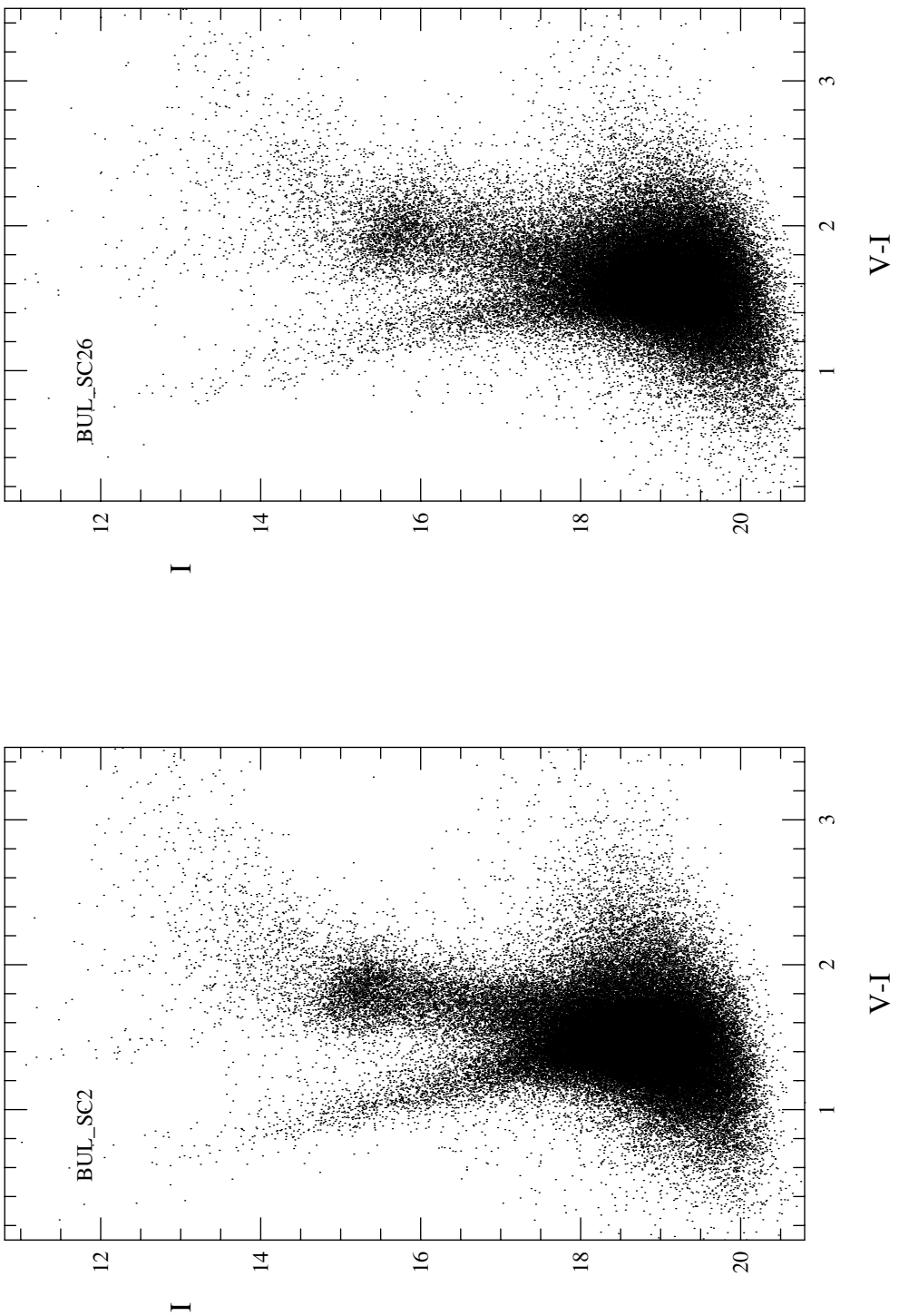

Fig. 13. Color-magnitude diagrams of the fields BUL_SC2 and BUL_SC26.

only the main sequence of disk stars is visible. In BUL_SC5, located somewhat farther from the center, the Galactic bulge red giant branch with highly elongated red clump becomes visible, but their large parts are still below the detection limit. Fig. 8 presents CMDs of two fields located about $1.^\circ 8$ from the Galactic center (BUL_SC37 and BUL_SC3). The interstellar extinction is much smaller than in the fields in Fig. 7 but it still changes significantly across the fields so the Galactic bulge red giant branch and red clump are severely smeared. In Fig. 9 CMDs of two additional fields from this group (BUL_SC4 and BUL_SC39) are shown. As the fields are farther from the Galactic center, the interstellar extinction becomes smaller and more uniform, although the variations across the fields are still significant. Fig. 10 presents CMDs of two fields located about $3.^\circ 2$ from the center. The fields (in particular BUL_SC22) cover regions with patches of higher extinction what again smears the red giant branch and red clump. CMD of BUL_SC43 field located at positive galactic latitude indicates as well high and non-uniform extinction on that side of the bulge while that of BUL_SC6 field located farther at negative latitudes shows much smaller and very uniform extinction (Fig. 11). Fig. 12 presents CMDs of two fields located in the Baade's window. Extinction in BUL_SC1 is much more uniform than in BUL_SC45. Finally, in Fig. 13 we plot CMDs of two fields (BUL_SC2 and BUL_SC26) located much further from the Galactic center in the regions of relatively small and uniform interstellar extinction.

8. Data Availability

The *VI* maps of the Galactic bulge are available to the astronomical community in the electronic form from the OGLE archive:

http://www.astrouw.edu.pl/~ogle
ftp://sirius.astrouw.edu.pl/ogle/ogle2/maps/bulge/

or its US mirror

http://bulge.princeton.edu/~ogle
ftp://bulge.princeton.edu/ogle/ogle2/maps/bulge/

Also *I*-band FITS template images of the OGLE-II fields are included. Total volume of the compressed data is equal to about 1.8 GB. Usage of the data is allowed under the condition of acknowledgment to the OGLE project with a reference to this paper.

We provide these data in the most original form to avoid any additional biases. For instance we do not mask bright stars which often produce many artifacts, but such a masking could potentially remove some interesting information on objects located close to them. We also do not remove objects which are located in overlapping areas between the neighboring fields. Cross-identification of these objects can be easily done based on provided equatorial coordinates.

Acknowledgements. We would like to thank Prof. Bohdan Paczyński for many discussions and help at all stages of the OGLE project. We thank Dr. D.S. Graff for information about the systematic error in the early OGLE calibrations. We also thank Dr. A. Olech for carrying out part of the observations of the Galactic bulge in the 1997 observing season. The paper was partly supported by the Polish KBN grant 2P03D01418 to M. Kubiak. Partial support for the OGLE project was provided with the NSF grants AST-9820314 and AST-0204908 and NASA grant NAG5-12212 to B. Paczyński. We acknowledge usage of The Digitized Sky Survey which was produced at the Space Telescope Science Institute based on photographic data obtained using The UK Schmidt Telescope, operated by the Royal Observatory Edinburgh.

REFERENCES

Bessell, M.S. 1990, *P.A.S.P.*, **102**, 1181.
Cardelli, J.A., Clayton, G.C., and Mathis, J.S. 1989, *Astrophys. J.*, **345**, 245.
Cordier, D., Lebreton, Y., Goupil, M.-J., Lejeune, T., Beaulieu, J.-P., and Arenou, F. 2002, *Astron. Astrophys.*, **392**, 169.
Dobrzycki, A., Groot, P.J., Macri, L.M., and Stanek, K.Z. 2002, *Astrophys. J. Letters*, **569**, L15.
Edge, W.R.T., and Coe, M.J. 2002, *MNRAS*, in press; astro-ph/0209327.
Eyer, L. 2002, *Acta Astron.*, **52**, 241.
Kurucz, R.L. 1993, *http://cfaku5.harvard.edu/*.
Landolt, A.U. 1992, *Astron. J.*, **104**, 372.
Paczyński, B., Udalski, A., Szymański, M., Kubiak, M., Pietrzyński, G., Soszyński, I., Woźniak, P., and Żebruń, K. 2000, *Acta Astron.*, **49**, 319.
Schechter, P.L., Saha, K., and Mateo, M. 1993, *P.A.S.P.*, **105**, 1342.
Subramaniam, A., and Anupama, G.C. 2002, *Astron. Astrophys.*, **390**, 449.
Szymański, M., and Udalski, A. 1993, *Acta Astron.*, **43**, 91.
Udalski, A., Kubiak, M., and Szymański, M. 1997, *Acta Astron.*, **47**, 319.
Udalski, A., Szymański, M., Kubiak, M., Pietrzyński, G., Woźniak, P., and Żebruń, K. 1998, *Acta Astron.*, **48**, 147.
Udalski, A., Szymański, M., Kubiak, M., Pietrzyński, G., Soszyński, I., Woźniak, P., and Żebruń, K. 2000, *Acta Astron.*, **50**, 307.
Woźniak, P.R., Udalski, A., Szymański, M., Kubiak, M., Pietrzyński, G., Soszyński, I., and Żebruń, K. 2002, *Acta Astron.*, **52**, 129.
Zaritsky, D., Harris, J., Thompson, I.B., Grebel, E.K., and Massey, P. 2002, *Astron. J.*, **123**, 855.